Supporting Information

Bandgap Engineering of Colloidal Zinc Oxysulfide via Lattice Substitution with Sulfur

Shiv K Pandey, Shipra Pandey, Vyom Parashar, Raghvendra S Yadav, G. K. Mehrotra, Avinash C Pandey

SYNTHESIS MECHANISM

Preferring to a recurrent strategy for solution-synthesis, composition modulated zinc oxysulfide ($ZnO_{1-x}S_x$ or ZOS) nanocrystals (NCs) with binary ZnO and ZnS have been synthesized through single-pot solution-combustion method. In a premeditated composition, ethanol and ethylene glycol is mixed in a ratio (4:1). A stoichiometric amount of zinc acetate is dissolved in above solution and heated at 60 ºC for 15 minutes. After that, an amount of thiourea (as a sulfur source), corresponding to requisite composition of ZOS is added to the above solution. The as prepared solution is placed in a furnace at 350 ºC for ignition. The solution mixture swelled up with liberation of the large amount of non-toxic fumes prompting highly exothermic combustion process. The resulting product is formed as fine yellowish-white powder. Similar experiments are repeated for synthesis of each composition with stoichiometric variation. Compare to other physical and chemical routes this method provides an effective channel to synthesize a series of ZOS compositions having high yield, low cost, stable and eco-friendly. The as synthesized products are characterized for their crystallographic formation, lattice strain calculations, TEM, SEM, EDAX, bandgap calculations and photoluminescence (PL) properties.

CHARACTERIZATION TECHNIQUES

X-ray diffraction (XRD) is performed on Rigaku D/max-2200PC diffractometer using CuKα1 radiation with wavelength of 1.5406 Å. HRTEM and SAED are carried out on Technai 30 G^2 S-Twin electron microscope operated at 300 kV. TEM imaging and STEM-EDS mapping of Zn, O and S elements is performed on JEOL, JEM 2100 electron

microscope operated at 200 kV using LaB_6 electron source. A relatively defocused convergent electron beam is raster scanned over an area of (512 x 512) pixel size with dwell time of 20 µS. High-resolution scanning electron microscopy (HRSEM) and EDAX measurements are performed on LEO FESEM 1530 Scanning electron microscope. Optical absorption properties are measured by Perkin-Elmer LS55 spectrophotometer. PL properties are studied using Perkin-Elmer Lambda35 spectrophotometer in the whole UV-visible range. X-ray photoelectron spectroscopy (XPS) measurements are performed on VSWESCA machine using Al-Kα (1486.6) X-rays under the vacuum pressure of 5×10^{-10} Torr.

STRAIN CALCULATIONS

The implicated lattice strain in ZOS compositions are plotted as a function of sulfur composition in figure 1.

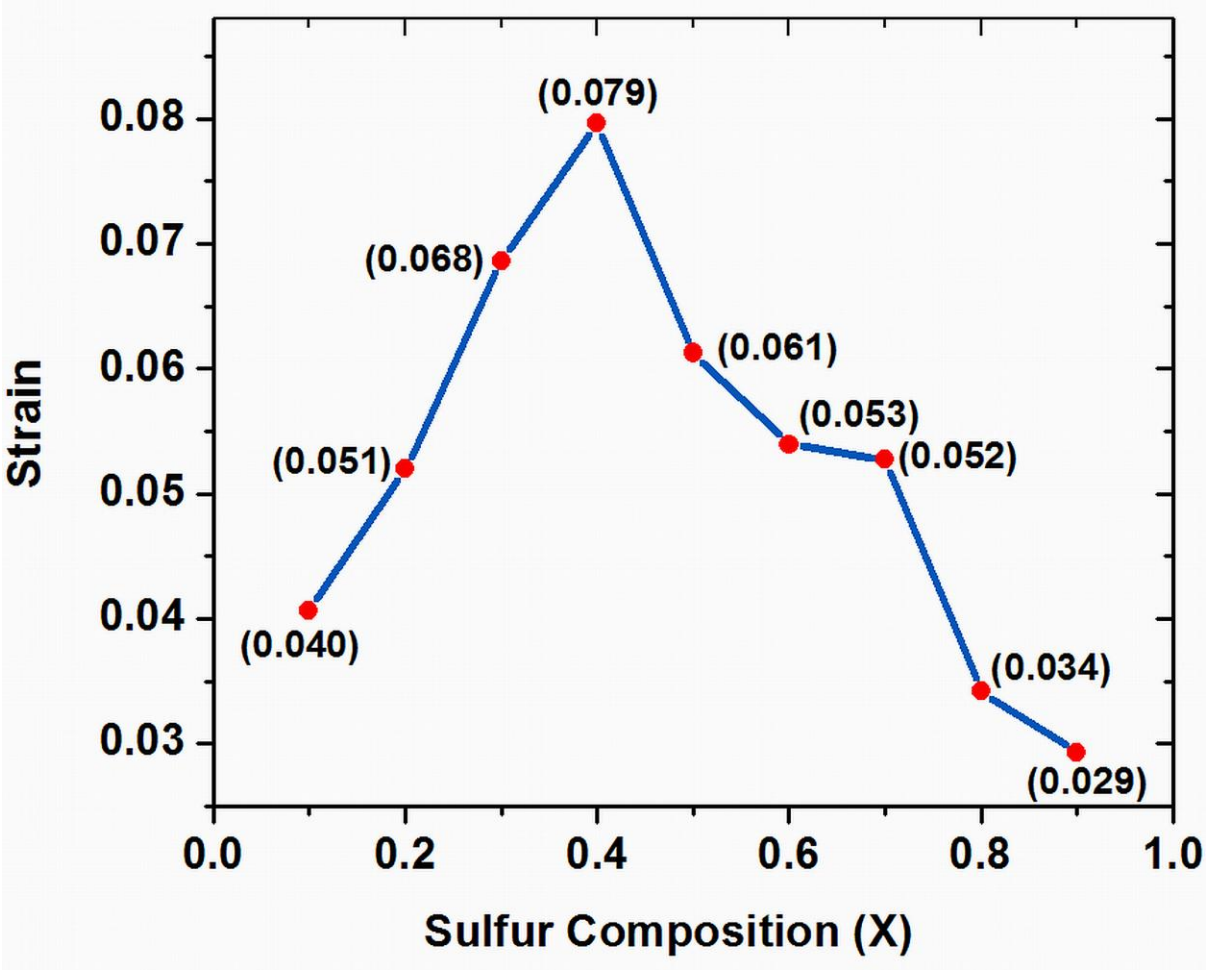

FIG. 1. Lattice strain in ternary composition as a function of sulfur. It shows an increase in strain up to 0.4 followed by subsequent decrease up to ZnS. It follows similar trends of anomalous bandgap variation and optical bowing parameter 'b'.

The calculations are performed for each composition using following equation-

$$\varepsilon = \beta / 4 \tan\theta$$

where ε is lattice strain, β is FWHM and θ is diffraction angle. In above shown graph, strain in lattice increases steeply and approximately becomes double in magnitude up to the composition of 0.4. A sharp decline is noticed for the composition 0.5 and afterwards. The decrease in lattice strain approaching towards ZnS becomes even lesser than ZnO probably due to less polar bonds between Zn and S relative to O. With raising S content, the size of ZOS NPs does not show any significant increase in particle size (micrographic studies) and therefore, small particle size and large lattice mismatch has synchronized contribution in lattice strain for each composition.[1] The strain induced variations has major contribution for the change in phase structure, absorption properties and PL properties.

X-RAY PHOTOELECTRON SPECTROSCOPY (XPS)

The figure 2 represents the X-ray photoelectron spectroscopy (XPS) analysis of the binary and representative ternary samples. A calibration of binding energy for each XPS spectrum is performed using C 1s at 286.98 eV.

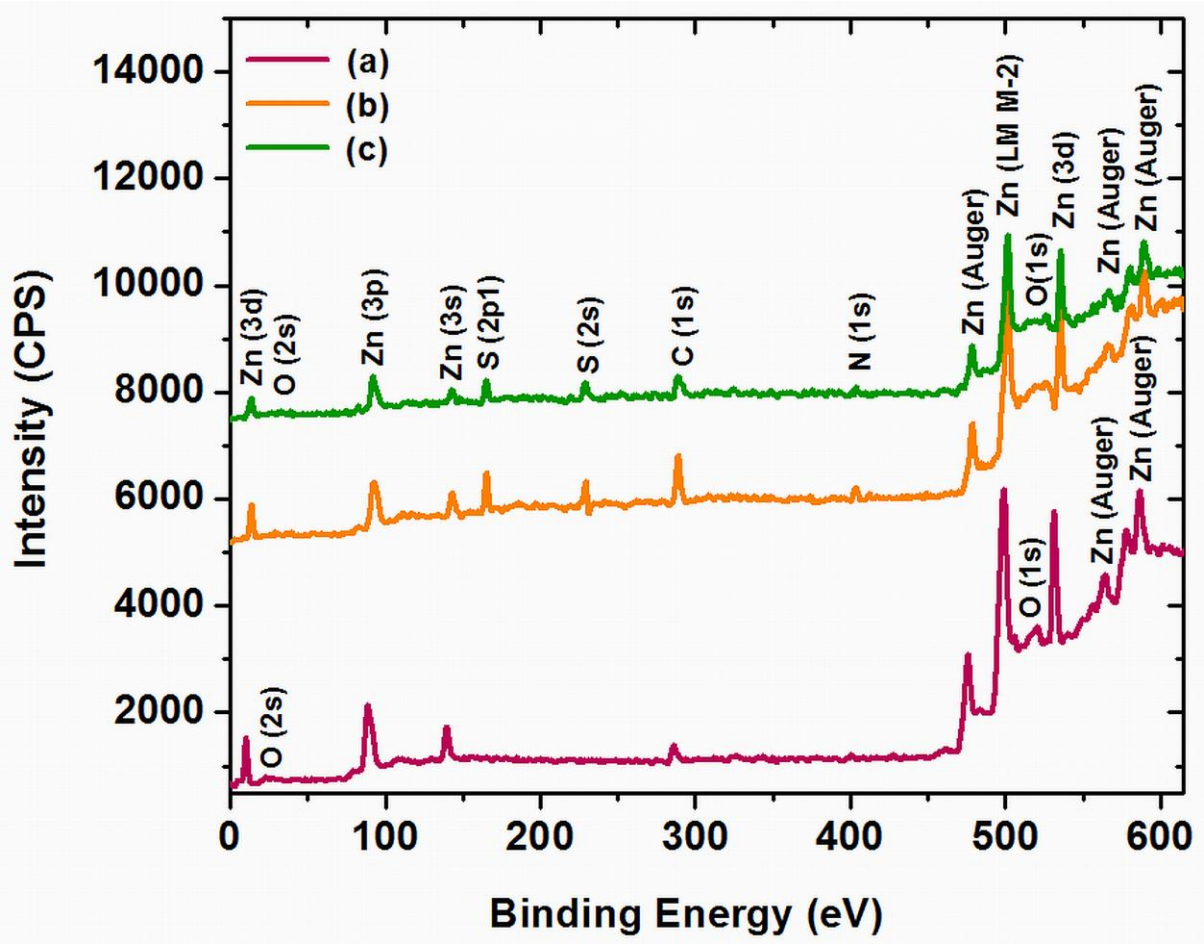

FIG. 2. Surface states analysis by XPS measurement revealing involved atomic orbital of Zn, O and S using binding energy as a function of hybridized states of atoms (a) ZnO; (b) ZOS (0.2) and (c) ZOS (0.4), respectively.

In figure 2a, a full range spectrum of ZnO reveals the contribution of various states of Zn and O. For the compositions 0.2 and 0.4 (figure 2b and 2c), Zn, O and S are identified corresponding to their binding energies. The binding energies of Zn 3d, Zn $3p\frac{1}{2}$ and Zn 3s are found at 14.04, 94.03 and 144.45 eV respectively. For both compositions, convoluted states of the sulfur, S 2p1 and S 2s are found at 165.31 eV and 229.65 eV individually.[2] The 2p1 component has binding energy of 165.31 eV, which is lower than sulfite ($-SO_3$), (166.4 eV) and sulfate ($-SO_4$) (168-170 eV), eliminating the possibility of these ions in these confirmations.[3] In figure 2a, O 2s and O 1s states are present at 23.34 eV (weak intensity) and 531.50 eV accordingly, while in the figure 2b and 2c spectra, O 2s state become insignificant and O 1s state at 535.66 eV decreases in intensity considerably. The O 1s peak at 535.66 eV could be attributed to the bonding between Zn Auger (580.87 eV) and S 2s (229.65 eV) states, which have comparable orbital (s and p) that can hybridize with appropriate energy.

An interesting disclosure validating XRD results is established with increasing sulfur concentration. Moreover, oxygen peaks have shown prominence up to thermodynamic solubility limit (TSL) of 30%, but as it processed over TSL, phase stability reverts toward ZnS with diminished oxygen peak intensity whereas of sulfur become prominent. This observation is found in accordance with composition variation. The absence of impurity peaks other than Zn, O, S, adsorbed carbon and nitrogen in XPS spectrum confirms the formation of pure phases of ZOS NCs.

TEM AND HRTEM ANALYSIS

The TEM and HRTEM images have been presented to validate the findings obtained from larger area.

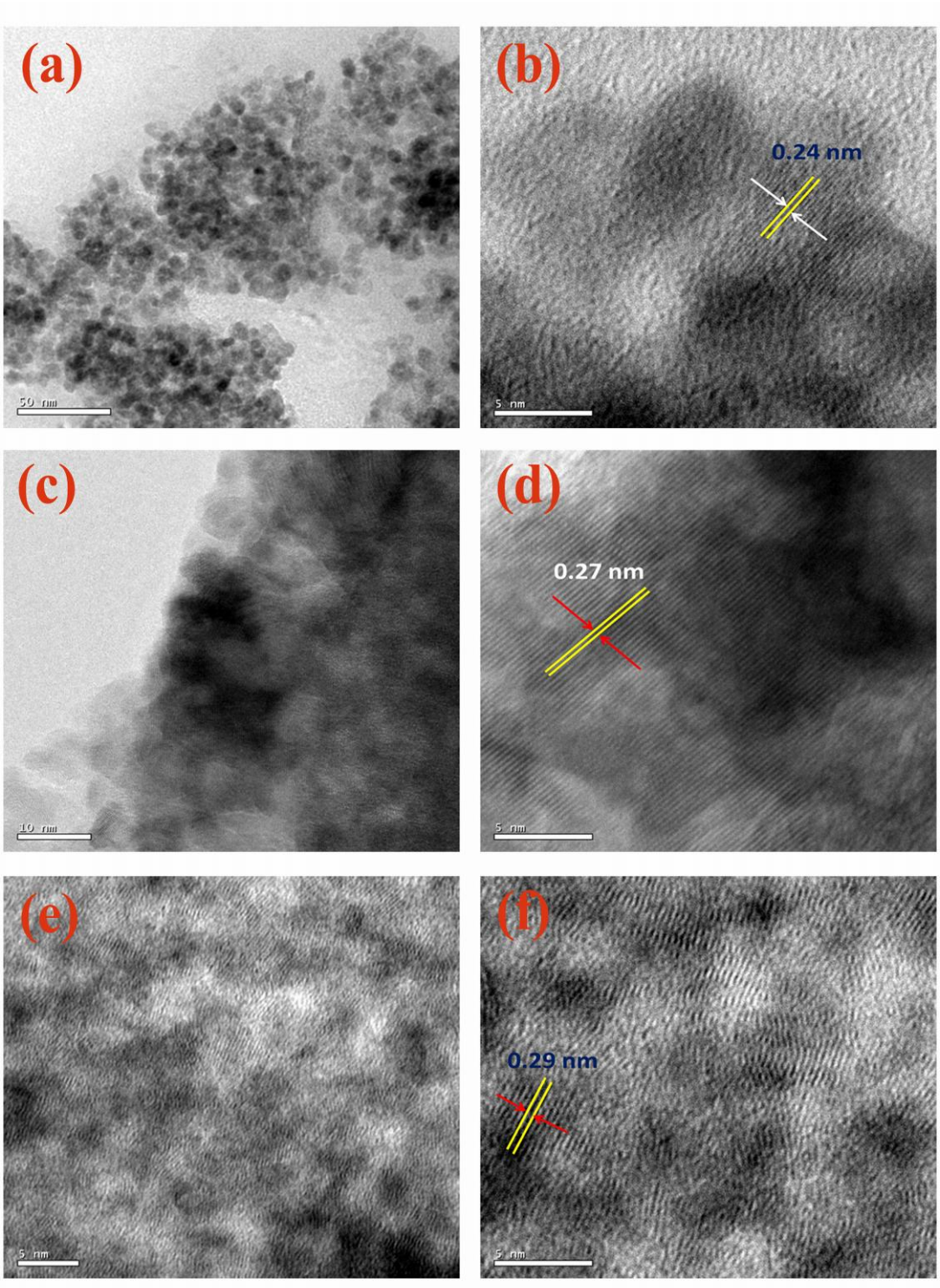

FIG. 3. Representative TEM images of ZnO (a (50 nm), b (5 nm)), ZOS (0.3) (c (10 nm), d(5 nm)) and ZnS (e (5 nm), f (5 nm)) respectively.

HRSEM AND EDAX ANALYSIS

HRSEM and EDAX studies have been performed to determine the morphology, chemical profiling and structural homogeneity of the representative ZOS (0.4) NCs. HRSEM images (figure 4a and 4b) have shown clumped ZOS compositions (0.4). An EDAX spectrum (figure 4c) from the circled position of above images reveals the elemental composition of Zn, O and S without other detectable elements that is substantiated as 37.50, 32.33 and 30.17 atomic% respectively, for the composition of 0.4.

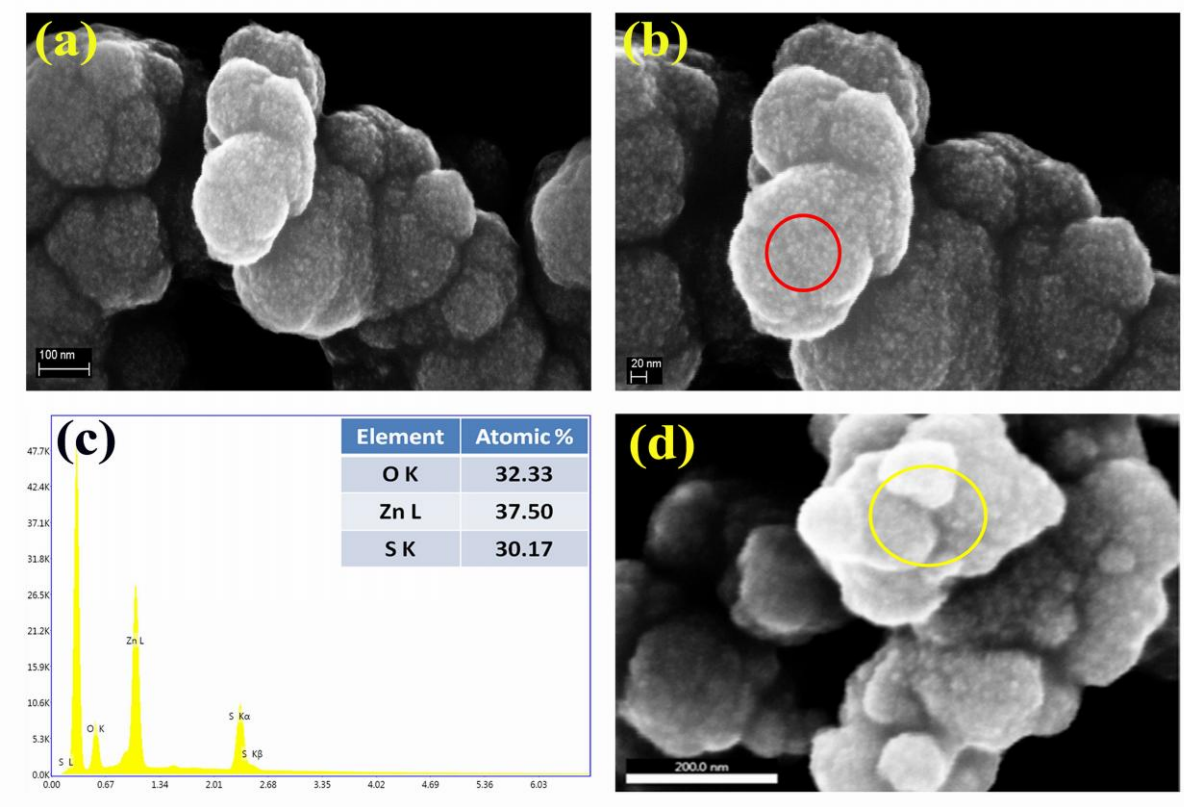

FIG. 4. HRSEM and Chemical profiling (EDAX) of ZOS NCs (4b) HRSEM images of ZOS (0.4); (4c) EDAX spectra obtained from the circled area in SEM image shows atomic composition; (4d)

The concentration of Zn is found in significantly lower concentration than sum of the O and S amount supports the existence of Zn vacancy in the sample (consistent with PL spectra).

BANDGAP CALCULATIONS

Table. SI (I) Bandgap, Bandgap bowing (b), index 'r' and type of transition for zinc oxysulfide nanoparticles

Composition (x%) of Sulfur in $ZnO_{1-x}S_x$	Bandgap Energy (eV)	Bandgap Bowing parameter (b)	Index (r)	Type of Transition
ZnO	3.74	0.00	1/2	Direct Allowed
$ZnO_{(0.9)}S_{0.1}$	3.37	4.43	3/2	Direct Forbidden
$ZnO_{(0.8)}S_{0.2}$	3.35	2.67	3/2	Direct Forbidden
$ZnO_{(0.7)}S_{0.3}$	3.30	2.36	3/2	Direct Forbidden
$ZnO_{(0.6)}S_{0.4}$	2.70	4.56	3/2	Direct Forbidden
$ZnO_{(0.5)}S_{0.5}$	2.77	3.66	3/2	Direct Forbidden
$ZnO_{(0.4)}S_{0.6}$	3.61	1.01	3/2	Direct Forbidden
$ZnO_{(0.3)}S_{0.7}$	3.81	0.34	3/2	Direct Forbidden
ZnS	3.93	0.00	1/2	Direct Allowed

In above table SI1, we have compiled the results obtained from the calculations of bandgap (E_g) energy, bowing parameter (b) and type of transition for each composition. The calculations for bandgap energies are discussed in absorption section and found the bandgap for each composition. Bowing parameter 'b' is calculated using equation-1 (in bowing parameter section) that has shown an inclination in 'b' up to 0.4 followed by declination. The various theoretical predictions have emphasized that numerical magnitude of 'b' for ZnS phases is higher than phases dominated by ZnO. Contrary to this, we found opposite results about 'b' values for ZnS compositions. Analyzing the factors for such observation we conclude that the values of 'b' follow the strain element that is bringing about to be highest for 0.4. Since 'b' value depends upon three entities; volume deformation, charge exchange and structural relaxation, it can be depicted that at 0.4, the degree of strain and therefore, bowing parameter should be utmost. The role of strain in the emission spectra can also be established that could be useful in determining the luminescence behavior of these NCs. An increase in single, sharp emission intensity peak is revealed from 0.1 to 0.4 followed by multiple, broad and random emission counts for further compositions. Analogous to other

factors like absorption, bowing etc. emission behavior for 0.4 compositions replicates manifold in terms of intensity due to removal of relaxation defect sites. An escalation and diminution in emission intensity are observed for all compositions respective of increase or decrease in lattice strain.

PHOTOLUMINESCENCE SPECTRA (PL)

Figure 5 illustrates the room temperature PL spectrum of the ZOS NCs compositions. We have used E_g absorption wavelength as an excitation source to their respective compositions. Emission intensities of the compositions (0.1 to 0.5) have been normalized to identify the peaks as emission intensity of initial compositions are too low to detect. Comparatively, subsequent compositions have shown emission intensity ten times brighter than binary components with tunable visible range emission.[4] In ZnO NCs, band-edge emission decreases drastically as it competes with deleterious surface traps.[5] Since, with increasing concentration of sulfur changes the bandgap of the ZOS composition (UV absorption study) therefore, it is obvious to change the corresponding emission position with manifold increase in emission intensity as sulfur passivates the deleterious surface defects and transfers the energy from non-radiative traps to the shifted band-edge.[6] For the subsequent compositions, as band-edge shifts with bandgap, a corresponding new emission positions are observed with enhanced emission intensity.

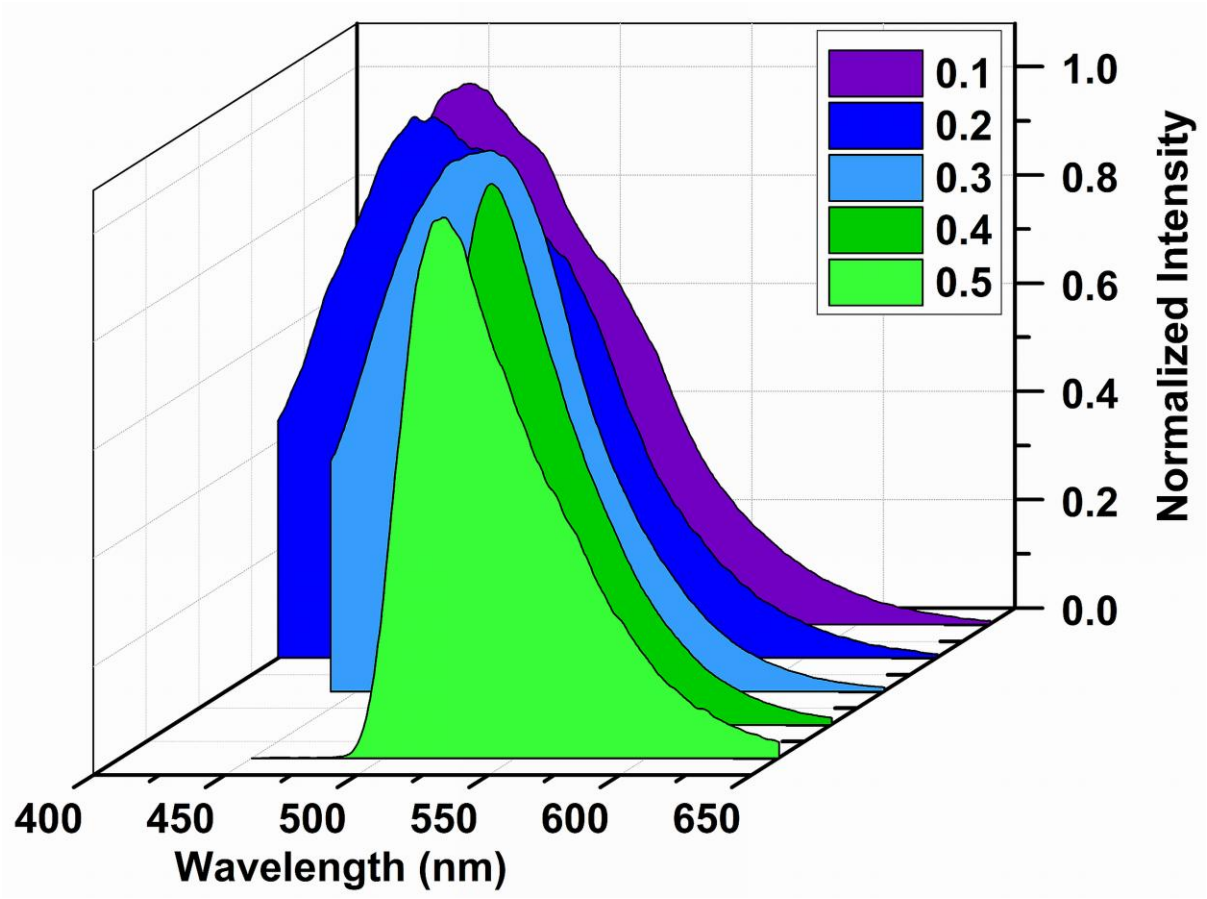

FIG. 5. PL spectra of ZOS for the compositions of (x= 0.1-0.5) exhibiting emission tunability in visible range at room temperature; An emission for composition 0.1 starts from violet region that stretches up to green emission (composition 0.5); excited wavelength λ_{exc}= absorbance peaks.

Incorporation of S with Zn and O significantly increases the irradiative efficiency due to enhanced energy transfer from band edge to defect states responsible for much brighter visible emission, reduced band edge emission, and faster band edge decay.[1,6,7,8,9] Accordingly, peak at 453 nm (x= 0.1) evolves due to passivation of deleterious traps of ZnO by S atoms that paved the way for energy transfer as irradiative emission from weak band-edge to defect states.[1,6,7] Similar emission peak is obtained at 458 nm (x= 0.2) with a broad shoulder at 509 nm that is due to lattice strain preventing relaxation sites to form defects traps.[1,6,7] Moreover, the broad and intense peak of this composition could be due to augmented oxygen vacancies. The broad green emission peak centered at 499 nm (x= 0.3) originates from recombination of holes with electrons occupying the singly ionized oxygen vacancies.[1,6,7] The viability of such emission is that the S in ZnO distorts the lattice structure which leads to the enhancement in green emission with usual suppression of UV band edge peaks providing evidence of presence of S with Zn and O in lattice. Another rationale of its presence is a sharp and intense yellowish-green emission at 521 nm (x= 0.4). Since,

increasing lattice strain with S directs the ease of relaxation to form defects trap sites, therefore elastic compression in lattice causes excellent emission properties.[1,6,7] The similar emission centered at 523 nm (x= 0.5) may be derived from some self activated centers, vacancy states or interstitial states.[10]

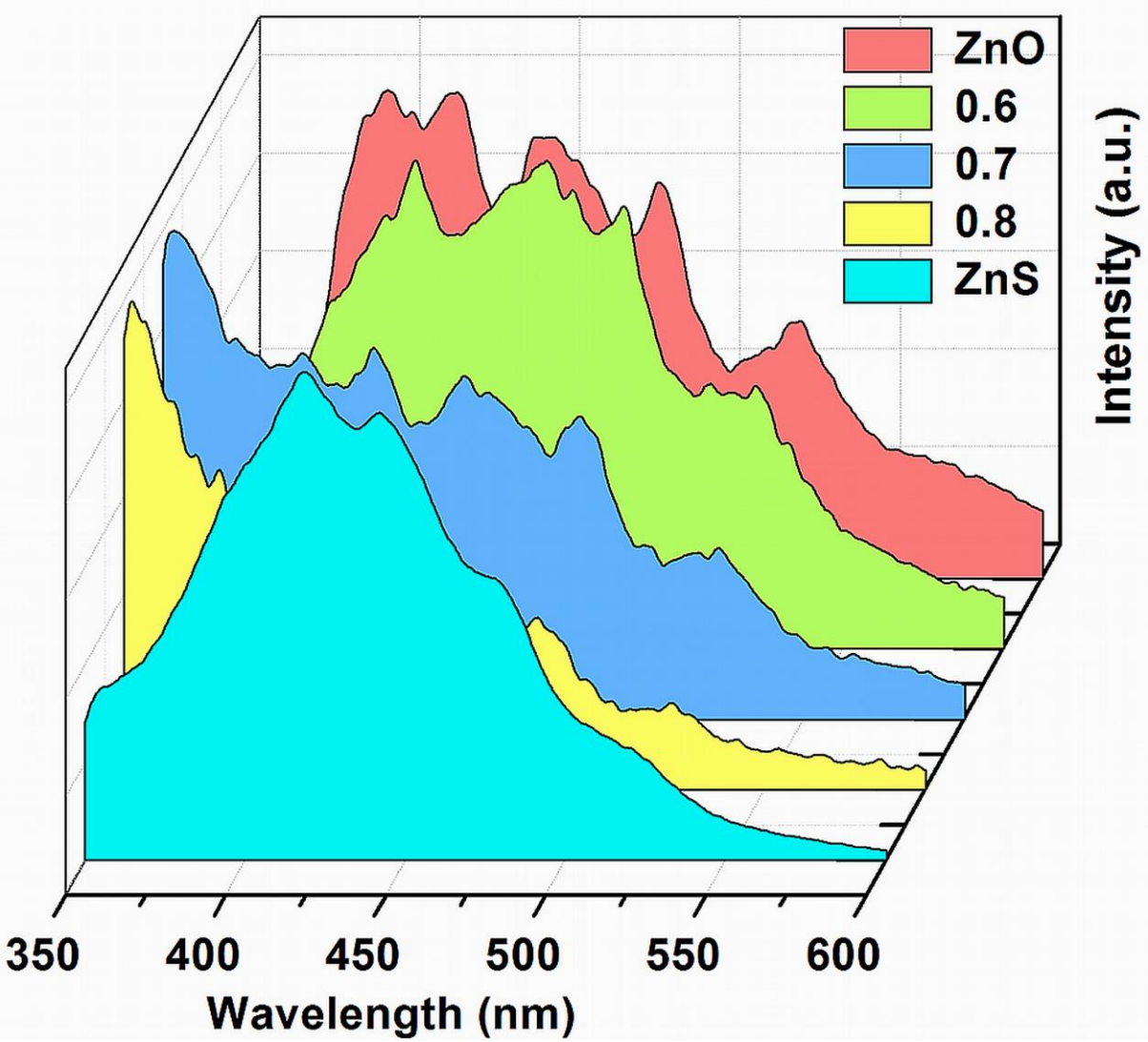

FIG. 6. PL spectra of ZnO and ZnS compounds with ZOS compositions (0.6 to 0.8) showing multiple emissions originated from defect dominated states

In figure 6, PL spectrum reveals the prominence of luminescence for the remaining compositions of ZOS with their binary oxides and sulfides. In ZnO, strong UV emission at 398 nm is originated from excitonic recombination of electrons and holes.[11] Similarly, abroad green spectrum at 524 nm may be derived from self-activated centers, vacancy states and interstitial states.[10,12] The emission of 481 nm in ZnO instigates from intrinsic surface defects.

Observation of strong blue emission at 418 nm (composition 0.6) relates to the suppression of UV band peak and enhancement of energy transfer from E_g to enriched surface defects in lattice due to increased sulfur concentration.[6] A broad emission peak at 483 nm is most likely corresponded to ZnS related luminescence of Zn vacancies.[13] For the composition 0.7 and 0.8, blue shift is observed probably due to increased charge carrier concentration provided by less electronegative S. Such gradual inclinations in charge carrier concentration lead to blue-shift in the optical band to band transition and known as "Burstein-Moss effect".[14] Weak emission spectra are obtained at 418 and 444 nm for binary ZnS. Though, the binary composition has also shown other emission peaks related to charge concentration, Zn vacancy or recombination of singly ionized vacancies, but they are much weaker than their alloyed compositions.

1. A. M. Smith, A. M. Mohs and S. Nie, *Nat. Nano.*, 2009, **4**, 56.
2. B. V. Crist, Handbooks of Monochromatic XPS spectra, **2**, Commercial binary pure oxides (XPS International), LLC, 2005, 952.
3. J. A. Rodriguez, T.Jirsak, S. Chaturvedi and M. Kuhn, *Surf. Sci.*, 1999, **442**, 400.
4. R. N. Bhargava, D. Haranath and A. Mehta, *J. Korean Phys. Soc.*, 2008, **53**, 2847.
5. I. Shalish, H. Temkin and V. Narayanmurthi, *Phys. Rev. B*, 2004, **69**, 245401.
6. J. V. Foreman, Y. H. Li, H. Y. Peag, S. Choi, H. O. Everitt and J. Liu, *Nano lett.*, 2006, **6**, 1126.
7. G. Shen, J. H. Cho, J. K. Yoo, G.-C. Yi and C. J. Lee, *J. Phys. Chem. B*, 2005, **109**, 5491.
8. S. Y. Bae, H. W. Seo and J. Park, *J. Phys. Chem. B*, 2004, **108**, 5206.
9. J. Tauc, R. Grigorovici and A. Vancu, *Phys. Status Solidi*, 1966, **15**, 627; A. Bhardwaj, E. Vardarajan, P. Srivastava and H. K. Sehgal, *Solid State Commun.*, 2008, **146**, 53; A. Abu El-Fadl, E. M. El-Maghraby and T. Yamazaki, *Cryst Res. Technol.*, 2008, **43**, 302.
10. T. Mitsni, N. Yamamoto, T. Tadokaro and S.-I. Ohta, *J. Appl. Phys.*, 1996, **80**, 6972.
11. J. Y. Lao, J. Y. Huang, D. Z. Wang and Z. F. Ren, *Nano Lett.*, 2003, **3**, 235; S. C. Lyu, Y. Zhang, C. J. Lee, H. Ruh and H. J. Lee, *Chem. Mater.*, 2003, **15**, 3294.
12. Y. Jiang, X. M. Meng, J. Lin, Z. Y. Xie, C. S. Lee and S. T. Lee, *Adv. Mater.*, 2003, **15**, 323.
13. W. H. Zhang, J. L. Shi, H. R. Chen, Z. L. Hua and D. S. Yan, *Chem. Mater.*, 2001, **13**, 648; A. L. Rogach, D. Nagesha, J. W. Ostrander, M. Giersig and N. A. Kotov, *Chem. Mater.*, 2000, **12**, 2676.
14. K. J. Kim and Y. R. Park, *Appl. Phys. Lett.*, 2001, **78**, 475.